Additive Effects on Si_3N_4 Oxidation/Volatilization in Water Vapor

Elizabeth J. Opila*[1], R. Craig Robinson*[2], Dennis S. Fox*, Richard A. Wenglarz[#], Mattison K. Ferber[&]

*NASA Glenn Research Center, Cleveland, OH 44135
[1]Cleveland State University, Cleveland, OH 44115
[2]QSS Group, Inc., Cleveland, OH 44135
[#]South Carolina Institute for Energy Studies, Clemson, SC 29634
[&]Oak Ridge National Laboratory, Oak Ridge, TN 37830

Abstract

Two commercially available additive-containing silicon nitride materials were exposed in four environments which range in severity from dry oxygen at 1 atm pressure, and low gas velocity to an actual turbine engine. Oxidation and volatilization kinetics were monitored at temperatures ranging from 1066 to 1400°C. The main purpose of this paper is to examine the surface oxide morphology resulting from the exposures. It was found that the material surface was enriched in rare earth silicate phases in combustion environments when compared to the oxides formed on materials exposed in dry oxygen. However, the in situ formation of rare earth disilicate phases offered little additional protection from the volatilization of silica observed in combustion environments. It was concluded that externally applied environmental barrier coatings are needed to protect additive-containing silicon nitride materials from volatilization reactions in combustion environments.

Introduction

Si_3N_4 is proposed for use as components, such as vanes, in turbine applications. Tens of thousands of hours of life are needed for both land-based turbines and aeropropulsion applications. Additive-containing Si_3N_4 materials are

proposed for these applications because they have the requisite toughness, strength, and creep resistance. Typical additives to Si_3N_4 are oxides such as Y_2O_3, La_2O_3, and other rare earth oxides. However, these additive-containing Si_3N_4 materials must also have enough oxidation resistance so that material recession does not limit the lifetime.

The oxidation resistance of these types of materials has been extensively studied in dry oxygen. It is well known that in dry oxygen, a silica scale forms that contains acicular grains of silicates such as $M_2Si_2O_7$ on the oxide surface (M=Y, La, etc. It was determined by Cubiciotti and Lau [1,2] that the outward diffusion of the additive cations (Y, La, Mg, etc.) controls the oxidation rate of these materials. The thermodynamic arguments for this mechanism have also been formulated [3].

Turbine environments are more complex. Water vapor is always present in the hot gas stream as a product of combustion. The oxidative durability of additive-containing Si_3N_4 in water vapor must therefore be understood. It was recently established that silica-forming materials undergo paralinear oxidation in water vapor environments [4-8]. Simultaneous oxidation of Si_3N_4 and volatilization of the silica scale occur by the following reactions.

$$Si_3N_4 + 6H_2O(g) = 3SiO_2 + 2N_2(g) + 6H_2(g) \quad (1)$$

$$SiO_2 + 2H_2O(g) = Si(OH)_4\,(g) \quad (2)$$

These combined reactions lead to accelerated rates of material consumption and recession.

For additive-containing Si_3N_4 oxidized in water vapor, it can be expected that the surface is simultaneously enriched in $M_2Si_2O_7$ silicates by outward cation diffusion and depleted in silica by volatilization in water vapor. It is then logical to ask whether it is possible to form an in situ continuous self-protective scale of $M_2Si_2O_7$, other silicates, or oxides which can lower the volatility rate of the scale, decrease the recession rate of Si_3N_4, and thereby increase the lifetime of these materials. The objective of this paper is to answer these questions for two types of commercially available additive-containing Si_3N_4, and to consider the implications of these results for all additive-containing Si_3N_4 materials.

Experimental Procedure

Material

The first material of study was AS800 Si_3N_4 (AlliedSignal Ceramic Components, Torrence, CA), an in situ reinforced β-Si_3N_4 containing a rare earth (RE)-based sintering system that results in a grain boundary phase of the apatite structure, $RE_{9.33}(SiO_4)_6O_2$. Some of the earlier AS800 material used in this work had RE silicon oxynitride grain boundary phases rather than the apatite phase. Chemical analysis by an inductively coupled plasma (ICP) technique shows the major additives are 4.2% La, 1.3% Y, and 1.0% Sr, by weight (wt%). The second material was SN282 (Kyocera Cermics, San Diego, CA). This material is also a β-Si_3N_4 containing Lu_2SiO_5 and $Lu_2Si_2O_7$ grain boundary phases. Chemical analysis, by ICP, indicates the SN282 contains 7 wt% Lu. For comparison, oxidation results under some conditions are also reported for high purity Chemically-Vapor-Deposited (CVD) Si_3N_4 without additives (Advanced Ceramics

Corporation, Cleveland, OH). This material is an α-Si_3N_4. Impurities in all three materials are described in reference [8].

Furnace testing – dry oxygen

Si_3N_4 coupons were oxidized in flowing dry oxygen (0.4 cm/sec) at one atmosphere total pressure and temperatures between 1200 and 1400°C for times up to 100h. Samples of 2.5 x 1.3 x 0.3 cm were suspended from a sapphire hanger in a fused quartz furnace tube. Weight change was acquired by a continuously recording microbalance. Further details can be found in Reference 8.

Furnace testing – wet oxygen

Si_3N_4 coupons were oxidized in flowing 50% H_2O/50 % O_2 by volume (4.4 cm/sec) at one atmosphere total pressure and temperatures between 1200 and 1400°C for times up to 100h. Sample size was the same as those exposed in dry oxygen. Samples were also suspended from a sapphire hanger in a fused quartz furnace tube. Weight change was acquired by a continuously recording microbalance. Details of the experimental setup and procedure can be found in References 4 and 8.

High Pressure Burner Rig (HPBR)

Si_3N_4 samples were exposed in the HPBR at NASA Glenn Research Center. Samples of size 7.6 x 1.3 x 0.3 cm were exposed to HPBR tests conducted at a fuel-to-air ratio of 0.063 using Jet A fuel. Typical test conditions consisted of total pressure equal to 6 atm, a gas velocity of 20 m/sec, material temperatures between 1150 and 1330°C, and a water vapor partial pressure of

about 12% or 0.7 atm. Exposure times were typically 50h, although some samples were tested for as long as 196h. Interrupted weight change measurements were acquired. Details of the experimental setup can be found in Reference 6.

Turbine engine

A demonstration of AS800 and SN282 first stage vanes was conducted at a large natural gas processing plant operated by Exxon near Mobile, AL as part of the Advanced Turbine Systems Program of the Department of Energy. One of three Rolls-Royce Allison 501-K turbines used to generate process steam from exhaust and provide electricity for the plant was retrofitted with ceramic vanes and associated mounts for the demonstration. Details of the project can be found in reference 9.

The average temperature and pressure of gas entering the vanes were about 1066°C and 8.7 atm. However, due to the combustor temperature pattern, the mid-span gas temperature was probably as high as 1260°C at the "hot spot". The inlet gas velocity at vane mid-span was about 161 m/sec and the gas accelerated to about 572 m/sec at the vane exit. The velocities for the AS800 vane examined in this study were somewhat distorted and probably somewhat lower because the vane was under the saddle, where lower oxidation rates were experienced. A water vapor content of 10.1% was calculated for the gas entering the vanes at the average ambient conditions for operation of the Exxon turbine (average of 29°C, 85 % relative humidity). The AS800 vanes were exposed in the test for 815 h. SN282 vanes were exposed for 1818 h.

Post-test analyses

The variation in scale composition and morphology with successively more severe exposure conditions (higher water vapor partial pressure and higher gas velocity) was examined by Scanning Electron Microscopy (SEM), Energy Dispersive Spectroscopy (EDS), and X-Ray Diffraction (XRD) analysis. The emphasis in this paper is on the development of the oxide scale composition and morphology. Oxidation and volatilization kinetics as determined by weight change, oxide thickness measurements, and surface recession are also mentioned, but are the subject of other papers.

Results

As-received material characterization

XRD analysis of the as-received AS800 showed β-Si_3N_4 and other phases that are presumed to be the grain boundary phase. In the older AS800 material, the grain boundary phase corresponded to known patterns for lanthanum silicon oxide nitride ($LaSiO_2N$, International Centre for Diffraction Data Powder Diffraction File (PDF) # 31-699), whereas in the newer batches of AS800, the grain boundary phase corresponded with cerium analogs of the apatite phase ($Ce_{4.667}(SiO_4)_3O$, PDF #43-441). XRD analysis of the as-received SN282 showed β-Si_3N_4 as well as the grain boundary phases Lu_2SiO_5 and $Lu_2Si_2O_7$.

Micrographs of the as-received materials can be seen in Figure 1. The long dark grains correspond to the β-Si_3N_4 whereas the bright phase is the rare earth-rich grain boundary phase. The grain size of the SN282 is finer than that of

the AS800. In general it is known that the AS800 has better mechanical properties whereas the SN282 has better oxidation resistance.

Furnace testing – dry oxygen

Oxidation rates for AS800, SN282, and CVD Si_3N_4 in dry oxygen, in the temperature range of 1200 to 1400°C, are the subject of another paper [8]. However, the results at 1300°C are summarized here in Table 1 for comparison to other tests. Oxidation rates for CVD Si_3N_4 were the lowest, followed by SN282, while those for AS800 were at least an order of magnitude larger than CVD Si_3N_4. In addition, the oxidation rates for AS800 showed variability from batch to batch.

XRD results for AS800 exposed at 1300°C for 100h showed β-Si_3N_4, cristobalite, and $La_2Si_2O_7$. XRD results for the scale formed at 1300°C in dry oxygen are shown in Figure 2 and compared with results at the same temperature under other conditions. The oxide morphology of AS800 exposed at 1300°C in Figure 3 showed a few regions containing larger acicular grains with aspect ratios up to 20. EDS analysis indicated these particles are consistent with $La_2Si_2O_7$.

XRD results for SN282 oxidized at 1300°C showed β-Si_3N_4, Lu_2SiO_7 and a trace of Lu_2SiO_5. These silicate phases were present in the grain boundaries of the as-received material, also. However, the SEM surface morphology in Figure 3 compared to the as-received material shown in Figure 1 clearly shows that a silica layer has formed and nearly spherical lutetium silicate particles are present on the surface.

Furnace testing – Wet oxygen

Oxidation kinetics for AS800, SN282, and CVD Si_3N_4 in wet oxygen are also described in detail in another paper [8]. The results obtained at 1300°C are summarized in Table 1. Under these conditions, paralinear oxidation was observed. Both oxidation rates and silica volatility rates have been determined from the weight change kinetics. Oxidation rates in water vapor were higher than those in dry oxygen as is true for silica formers in general [10,11]. The relative ranking of the oxidation rates of the three materials is the same as that found in dry oxygen: CVD Si_3N_4 the lowest and AS800 the highest. Volatility rates are in relative good agreement with rates observed for silica volatility. Although, statistically the rates were not significantly different, the average value of volatility rate was highest for CVD Si_3N_4, followed by AS800, with SN282 the lowest.

XRD results for AS800 oxidized at 1300°C in 50% water vapor/50% oxygen showed formation of cristobalite and $La_2Si_2O_7$ (Figure 2). The SEM surface morphology was similar in appearance to samples oxidized in dry oxygen. However, as shown in Figure 4, for areas near the bottom of the coupon where the gas boundary layer is thinnest and the gas velocity is highest, a porous oxide is visible which is enriched in La (presumably as $La_2Si_2O_7$) relative to other areas of the coupon.

XRD results for SN282 exposed at 1300°C in 50% water vapor/50% oxygen showed formation of cristobalite and $Lu_2Si_2O_7$. Surface SEM, Figure 5, showed that silica formed with a fine dispersion of nearly spherical $Lu_2Si_2O_7$ particles on the surface. The distribution of these surface particles corresponded

to the distribution of the grain boundary phase in the as-received material (Figure 1). This contrasts with the more sparse distribution of $Lu_2Si_2O_7$ particles observed for samples oxidized in dry oxygen.

HPBR

Oxidation rates for Si_3N_4 materials in the HPBR are only measurable for AS800 due to the relatively high oxidation rate of this material. AS800 exhibited paralinear behavior with initial weight gains followed by nearly linear weight loss. Oxidation rates were obtained by fitting the weight change kinetics to the paralinear weight change equation as in Reference 4. CVD Si_3N_4 and SN282 showed weight losses at the first weight change measurement due to the much lower oxidation rates of these materials relative to silica volatility rates. Therefore only linear volatility rates are reported for these materials. The weight loss rates for all three materials are shown in Figure 6 as a function of temperature. A comparison of the AS800 and SN282 weight loss rates with the CVD Si_3N_4 shows that additives do not significantly lower volatility rates. The weight loss rates appear highest for AS800 followed by CVD Si_3N_4. The weight loss rates of SN282 are about a factor of two lower than those of AS800 at the same temperatures. Most data points in Figure 6 reflect 50h exposures. However, the two large data points for AS800 at the low and high temperatures were for 186 and 196h respectively. These points demonstrate that the linear weight loss rates of AS800 did not slow down at longer times despite the surface enrichment of the rare earth disilicate phase.

XRD results for AS800 exposed in the high pressure burner rig at 1300°C for 50h show the formation of cristobalite and $La_2Si_2O_7$ (Figure 2). In addition, the major peak for yttria is present. SEM (Figure 7) shows significant coarsening of the acicular grains of $La_2Si_2O_7$ on the surface as well as a much higher surface coverage of this phase compared to the surface morphology for materials oxidized in the furnace exposures at the same temperature (Figures 3 and 4).

EDS spot analysis shows three phases on the surface. The EDS results for the large acicular grains are consistent with $La_2Si_2O_7$, however a strong Y peak is always present for these grains. Y is only detected in the presence of La, Si, and O, indicating that pure Y_2O_3 is not present. It seems likely that the $La_2Si_2O_7$ grains have an effective composition of $(La,Y)_2Si_2O_7$. A similar phase has been previously reported by Monteverde et al. [12] although the results obtained here did not fit the reported XRD pattern. In addition, the observed XRD pattern was not in exact agreement with the powder diffraction file for $La_2Si_2O_7$, but showed some d-value changes as would be expected for Y substitution on a La site. The possibility of a partially yttrium substituted $La_2Si_2O_7$ phase, however, is inconsistent with the XRD results that showed the highest intensity peak for Y_2O_3.

The second phase observed by EDS, the continuous medium contrast phase, is also enriched in La. Impurities found in the burner rig, such as calcium, concentrate in this phase. This phase also appears to be liquid or of low viscosity at the test conditions probably due to formation of low temperature

eutectics with impurities. Finally, nearly round dark areas are observed that are indicated to be nearly pure SiO_2 by EDS.

XRD results for SN282 exposed in the HPBR at 1225°C for 102h indicate $Lu_2Si_2O_7$ plus minor amounts of cristobalite and Lu_2SiO_5. SEM in Figure 8 shows surface enrichment of the $Lu_2Si_2O_7$, however, not to as great an extent as observed for the AS800 at 1300°C.

Cross-sectional SEM of the materials exposed in the HPBR, shown in Figure 9, gives additional information for evaluating the protective qualities of the oxide scales. Figure 9A shows AS800 exposed in the HPBR at 1170°C for 50h. Two features are of note. First, spalling of the $La_2Si_2O_7$ layer is evident. The acicular grains are barely adherent to the underlying material. Second, subsurface damage is observed, including both subsurface oxidation and cracking. The low temperature liquid phase is not observed. At higher temperatures (1330°C), as in Figure 9B, the low temperature liquid phase is observed. However, peaks of silica, as noted by the arrows, project out of the surrounding melt. This phase, therefore, offers no protection to the silica. In Figure 9C, another section of the sample exposed at 1330°C, showing the best coverage by $La_2Si_2O_7$, is shown. Here, at high magnification it can be seen that both through thickness cracks and cracks in the $La_2Si_2O_7$ parallel to the silica interface are found, as noted by the arrows. The possible origin of these cracks will be discussed later. Finally, in Figure 9D, a cross-section of SN282 exposed in the HPBR at 1225°C for 102 h is shown. The cross-section shows stalks of SiO_2 with $Lu_2Si_2O_7$ caps on top. The areas between the $Lu_2Si_2O_7$ show much

thinner silica layers. The area in Figure 9D shows the largest continuous section of $Lu_2Si_2O_7$ observed for this sample cross-section. In this material, the rare earth disilicate shows protection of the underlying silica where it is present on the surface.

Turbine vanes

Measured recession values of AS800 and SN282 turbine vanes are reported in Figure 10. The large scatter in recession can be attributed to variations in temperature seen for different vanes throughout the turbine. The recession rate of SN282 is about half that of AS800 vanes if lines are drawn through the points of maximum recession for each material. This is consistent with the weight loss results from the HPBR reported above.

XRD analysis of AS800 vanes varied. One vane positioned in the saddle of the turbine showed bare Si_3N_4 with La_2O_3. This pattern is shown in Figure 2. XRD of other vanes are reported to show $La_2Si_2O_7$ or accumulated grain boundary phase [13]. SEM of vane cross-sections showed a bare surface for the vane in the saddle position (Figure 11A) while a cross-section of another vane showed subsurface grain boundary damage (Figure 11B). This damage is consistent with damage observed in the HPBR at 1170°C. Cross-sectional SEM of an SN282 vane showed accumulation of $Lu_2Si_2O_7$ at the vane surface (Figure 12). The $Lu_2Si_2O_7$ does not appear to be adherent, however, the particles have still accumulated despite the high gas velocities in the turbine, so some adherence must be maintained.

Discussion

The selective volatilization and surface enrichment of rare earth disilicates for additive containing Si_3N_4 in combustion environments has been demonstrated for both AS800 and SN282, especially when comparing the results obtained for exposures in dry oxygen to those obtained in the high pressure burner rig. However, the rare earth disilicates do not remain adherent in the extreme conditions of the turbine. Factors that affect the optimization of in situ formation of adherent protective rare earth disilicate surface layers will now be discussed, both in terms of the two materials examined in this paper and for additive-containing silicon nitrides in general. These factors include rare earth cation mobility effects, thermal expansion match among the rare earth disilicate and Si_3N_4 and SiO_2, the phase stability of rare earth disilicates, and finally, the silica activity of rare earth disilicates.

Cation mobility effects

Surface enrichment of the oxide scale with the rare earth disilicates is first dependent on the exposure temperature. Lee and Readey [14] have demonstrated for Yb_2O_3 additions in Si_3N_4 (Kyocera SN362) that the grain size and surface coverage of the rare earth disilicates is more strongly dependent on temperature than on exposure time for oxidation in air at temperatures between 1250 and 1500°C. This suggests that rare earth cation mobility is very strongly dependent on temperature, especially when compared to the temperature dependence for oxidation of pure silica formers.

A second consideration of cation mobility effects is the variation between mobility of the various rare earth cations. The rare earth series in the periodic table extends from lanthanum, (the primary additive in AS800) which is the lightest with the largest ionic radius, to lutetium, (the primary additive in SN282) which is the heaviest and has the smallest ionic radius. It is expected that the cation mobility would increase as the ionic radius decreases so that more lutetium silicates would form than lanthanum silicates. However, the grain boundary phases in the two materials studied here are different (the apatite phase is not stable in the Lu_2O_3-SiO_2 system) and in fact the opposite effect is observed.

As mentioned in the introduction, the oxidation rate for additive-containing Si_3N_4 has been found to depend on the rate of cation diffusion outward. In AS800 the variability in oxidation rates may be partially explained by the variation in observed grain boundary phase. Diffusion of lanthanum outwards may be more rapid in the oxynitride phase than in the apatite phase, or vice versa. In addition, the relatively higher surface enrichment of rare earth silicates observed for AS800 compared to SN282 can be attributed to the ease of transport of rare earth cations through the grain boundary phase. For AS800, this transport rate would be substantially increased at temperatures over 1300°C where the liquid (or low viscosity phase) is formed. If the formation temperature of the liquid phase varies from sample to sample this could also explain the large scatter in oxidation rates observed at 1300°C. In designing an additive containing material for best oxidation/volatilization performance, the goal would be to chose a rare

earth cation/grain boundary phase system in which the balance between promotion of the surface silicate formation for volatilization protection and the prevention of grain boundary depletion and degradation is optimized.

Thermal Expansion Mismatch

Given the goal of in situ development of a protective rare earth disilicate surface phase, a good match of thermal expansion among the rare earth disilicate, Si_3N_4, and SiO_2 is needed. The CTEs (Coefficients of thermal expansion) for Si_3N_4 and cristobalite are relatively close. These materials have shown good cyclic oxidation behavior in air, indicating that oxide spallation is not an issue in the absence of water vapor enhanced surface enrichment of rare earth disilicates [15]. However, the cracks, both through thickness and at the phase interface seen in Figure 9C, show that some CTE mismatch between rare earth disilicate and the Si_3N_4/SiO_2 system may exist. Unfortunately, CTE values for the rare earth disilicates were not found in the open literature. Determination of these values would be useful in designing a rare earth additive containing Si_3N_4 for in situ growth of an adherent rare earth disilicate scale.

Phase stability

Another possibility for the cracks observed in Figure 9C could be phase instability of the rare earth disilicate. It is known that many structural polymorphs exist for the rare earth disilicates [16]. Figure 13 shows the regions of stability of seven crystal structures as a function of ionic radius and temperature. All phase transitions occur between 1200 and 1500°C, a temperature range that unfortunately coincides with the use temperature of the additive containing silicon

nitrides. Felsch concludes that all transitions between polytypes are reconstructive in nature. Volume changes are associated with the transitions. These transitions might explain the cracks observed in the $La_2Si_2O_7$ in Figure 9C. $Lu_2Si_2O_7$ and $Yb_2Si_2O_7$, in contrast, maintain the same polymorph from room temperature to the melting point of the compounds. For phase stability, the rare earths Lu and Yb are clearly most desirable as additives for Si_3N_4.

Silica activity in rare earth disilicates

A nonideal low silica activity is desirable if the rare earth disilicate is to offer protection from volatility for additive-containing Si_3N_4. In a water vapor environment, silica will be selectively volatilized from a silicate compound leaving a porous oxide. This effect has been observed for mullite ($3Al_2O_3 \bullet 2SiO_2$) coatings on SiC [17]. The silica activity in mullite is nearly ideal, 0.3 to 0.4. After exposure in the high pressure burner rig, silica was volatilized from the mullite, leaving a layer of porous alumina on the surface of mullite. Volatility rates in the HPBR for mullite coated SiC were only slightly reduced compared to uncoated SiC [17].

The phase diagram for the $La_2O_3 - SiO_2$ system is shown in Figure 14. The silica activity in the phase field $La_2Si_2O_7 + SiO_2$ must equal one. Therefore, any time the surface RE disilicate is in contact with silica, the silica activity of the RE disilicate is one. No reduction in volatility rate is expected, in this case, by the formation of the RE disilicate on the surface of the silica scale. However, where the surface is depleted in silica, or where the RE disilicate is not in contact with silica, there may be some reduction in silica activity and therefore some

reduced volatility by $Si(OH)_4(g)$ formation. How low can the silica activity in a rare earth disilicate be? In the $La_2O_3 - SiO_2$ system, Bondar [18] gets good agreement between experimental and calculated values of the liquidus near the La_2O_3-rich eutectic *when assuming ideal solutions of the initial oxides*. This suggests that the silica activity in the compound La_2SiO_5 is nearly ideal and the silica activity in the $La_2O_3 - SiO_2$ system is approximately ideal across the phase diagram. The largest reduction in silica activity to be expected is thus equal to the mole fraction of silica in the compound. The rare earth disilicate in this system will thus have a silica activity and a volatility rate of two-thirds that of pure silica. Clearly, a lanthanum disilicate layer on the surface of additive-containing silicon nitride is expected to offer little reduction in silica volatility over that observed for a pure silica scale. This is in agreement with the results obtained for AS800 in the water vapor furnace exposure, the high pressure burner rig and in the industrial turbine.

A phase diagram for the Lu_2O_3 - SiO_2 system has not been found in the literature, although the one for the Yb_2O_3 - SiO_2 system (next smallest RE cation) is available. Although the apatite phase is not stable in this system, most of the phase diagram is quite similar to that of the La_2O_3 - SiO_2 system. It is expected that the silica activity across the diagram would be similarly ideal. Experimentally, it is seen that the volatility and recession rates of SN282 are reduced by about a factor of two compared to pure silica. This could be explained if the silica activity in $Lu_2Si_2O_7$ is found to be slightly less than ideal. However, the silica activity must be orders of magnitude lower in order for

volatility rates to be reduced to acceptable levels [6]. Clearly, the in situ formation of a dense adherent rare earth disilicate surface layer on additive-containing Si_3N_4 is insufficient protection for these materials in combustion environments.

The enrichment of the oxide surface formed on silicon nitride in a low silica-activity phase, perhaps by further depletion of the rare earth disilicate to a stable rare earth oxide, is conceptually possible. As seen in the case of mullite, however, the depletion of silica from mullite resulted in the in situ formation of a porous alumina surface layer. The prospect of a porous layer remaining adherent in a high velocity environment is unlikely. In this study, XRD analysis of an AS800 vane exposed in the turbine showed the formation of La_2O_3, though an adherent oxide layer was not observed on the surface.

Because in situ formation of a protective layer does not significantly decrease volatility-induced recession, Environmental Barrier Coatings (EBC's) will be required for long-term application of additive containing silicon nitrides in combustion environments. Much work has been devoted to the development of these coatings. A summary can be found in reference 19. Externally applied rare earth silicates have been shown to offer some protection for silica forming materials [20], however, the stability of this class of coatings in combustion environments need to be further explored.

Summary and Conclusions

Silica is selectively volatilized from the oxide scale formed on additive-containing silicon nitrides exposed in combustion environments. Rare earth

disilicate enrichment is observed on the surface of these exposed materials, but it is not uniform. CTE mismatch and/or phase stability can cause spallation of the surface rare earth disilicate. Self-protecting silicate formation is not observed for AS800 or SN282, but a factor of two reduction in volatility and recession had been observed for SN282. Protection of additive-containing Si_3N_4 by optimized in situ formation of rare earth disilicate phases is likely to provide only a slight decrease in volatility and associated recession due to the high silica activities of rare earth disilicate phases. Externally applied environmental barrier coatings are necessary for use of additive-containing Si_3N_4 in combustion environments.

Acknowledgments

The authors would like to thank the following: Ralph Garlick of NASA Glenn Research Center conducted the XRD analyses. QuynhGiao N. Nguyen also of NASA Glenn Research Center provided some of the furnace exposure results. Susan Lewton, currently a student at Purdue University, also provided some of the furnace exposure and SEM results.

References

1. D. Cubiciotti and K.H. Lau, "Kinetics of Oxidation of Hot-Pressed Silicon Nitride Containing Magnesia," J. Am. Ceram. Soc. 61 [11-12] 512-517 (1978).
2. D. Cubiciotti and K.H. Lau, "Kinetics of Oxidation of Yttria Hot-Pressed Silicon Nitride," J. Electrochem. Soc. 126 [10] 1723-1728 (1979).
3. D.R. Clarke, "Thermodynamic Mechanism for Cation Diffusion through and Intergranular Phase: Application to Environmental Reactions with

Nitrogen Ceramics," pp. 421-426 in Progress in Nitrogen Ceramics, ed. F.L. Riley, Martinus Nijhoff Publishers, The Hague, The Netherlands, 1983.

4. E.J. Opila, R.E. Hann, "Paralinear Oxidation of CVD SiC in Water Vapor," J. Am. Ceram. Soc., 80 [1] 197-205 (1997).
5. J.L. Smialek, R.C. Robinson, E.J. Opila, D.S. Fox, N.S. Jacobson, "SiC and Si_3N_4 Recession due to SiO_2 Scale Volatility under Combustor Conditions," Adv. Composite Mater., 8 [1] 33-45 (1999).
6. R.C. Robinson and J.L. Smialek, "SiC Recession due to SiO_2 Scale Volatility under Combustion Conditions. Part I: Experimental Results and Empirical Model," J. Am. Ceram. Soc. 82 [7] 1817-25 (1999).
7. E.J. Opila, J.L. Smialek, R.C. Robinson, D.S. Fox, and N.S. Jacobson, "SiC Recession due to SiO_2 Scale Volatility under Combustion Conditions. Part II: Thermodynamics and Gaseous Diffusion Model," J. Am. Ceram. Soc. 82 [7] 1826-34 (1999).
8. D.S. Fox, E.J. Opila, Q.N. Nguyen, D.L. Humphrey, S.M. Lewton, "Paralinear Oxidation of Silicon Nitride in a Water Vapor/Oxygen Environment," submitted to J. Am. Ceram. Soc.
9. R.A. Wenglarz and K. Kouns, "Ceramic Vanes for a Model 501-K Industrial Turbine Demonstration," ASME IGTI paper 2000-GT-73.
10. B.E. Deal and A.S. Grove, "General Relationship for the Thermal Oxidation of Silicon," J. Appl. Phys. 36 [12] 3770-3778 (1965).
11. E.J. Opila, "The Variation of the Oxidation Rate of Silicon Carbide with

Water Vapor Pressure," J. Am. Ceram. Soc., 82 [3] 625-36 (1999).

12. F. Monteverde and G. Celotti, "Structural Data from X-ray Powder Diffraction of a New Phase Formed in the Si_3N_4-La_2O_3-Y_2O_3 System After Oxidation in Air," J. Eur. Cer. Soc. 19 [11] &2021-2026 (1999).
13. M.K. Ferber, H.T. Lin, V. Parthasarathy, and R.A. Wenglarz, "Degradation of Silicon Nitirdes in High Pressure, Moisture Rich Environments, " ASME IGTI paper 2000-GT-0661.
14. S.K. Lee and M.J. Readey, "Development of a Self-Forming Ytterbium Silicate Skins on a Silicon Nitride by Controlled Oxidation," J. Am. Ceram. Soc., 85 [6] 1435-1440 (2002).
15. E.J. Opila, D.S. Fox, and C.A. Barrett, "Cyclic Oxidation of Monolithic SiC and Si_3N_4 Materials," Cer. Eng. Sci. Proc. 14 [7-8] 367-374 (1993).
16. J. Felsche, "Polymorphism and Crystal Data of the Rare-Earth Disilicates of Type $R.E._2Si_2O_7$," J. Less Common Metals 21, 1-14 (1970).
17. K.N. Lee, "Key Durability Issues With Mullite-Based Environmental Barrier Coatings for Si-Based Ceramics," Trans. ASME 122, 632-636 (2000).
18. I.A. Bondar, "Rare-Earth Silicates," Cer. Int. 8 [3] 83-89 (1982).
19. K.N. Lee, D.S. Fox, J.I. Eldridge, D. Zhu, R.C. Robinson, N.P. Bansal, and R.A. Miller ,"Upper Temperature Limit of Environmental Barrier Coatings Based on Mullite and BSAS, " this issue.
20. T. Fukudome, S. Tsuruzono, W. Karasawa, Y. Ichikawa, "Development and Evaluation of Ceramic Components for Gas Turbine, "ASME Turbo

Expo 2002, June 3-6, 2002, Amsterdam, The Netherlands, GT-2002-30627.

Tables

Table 1. Comparison of oxidation/volatilization rate constants at 1300°C

	CVD Si_3N_4	**AS800**	**SN282**
	parabolic oxidation rate constant (mg^2/cm^4 h)		
dry O_2	$1.6x10^{-5}$	$3.4x10^{-4}$	$5.5x10^{-5}$
50% H_2O/50% O_2	$3.5x10^{-4}$	$8.6x10^{-4}$	$4.2x10^{-4}$
HPBR	--	$5.5x10^{-2}$	--
turbine	--	--	--
	linear volatilization rate constant (mg/cm^2 h)		
50% H_2O/50% O_2	$6.5x10^{-3}$	$4.2\ x10^{-3}$	$2.0x10^{-3}$
HPBR	$5x10^{-2}$	$6.3x10^{-2}$	$3.2x10^{-2}$ *
turbine	--	$2.4x10^{-1}$ *	$1.2x10^{-1}$ *

*Temperatures less than 1300°C

Figures

1. SEM images of the as-received materials. A) AS800 B) SN282
2. XRD spectra for AS800 exposed under various conditions. The O_2, H_2O, and HPBR exposures were obtained at 1300°C. The turbine exposure was at temperatures between 1066 and 1260°C.
3. SEM images of AS800 (A) and SN282 (B) surfaces after exposure in dry oxygen at 1300°C for 100h.
4. SEM images and corresponding EDS analyses of AS800 surfaces after exposure at 1300°C, 0.5 atm H_2O, 4.4 cm/s, for 100h. (A) typical area (B) bottom of sample.
5. SEM image of SN282 surface after exposure at 1300°C, 0.5 atm H_2O, 4.4 cm/s, for 100h.
6. Weight loss rates obtained for Si_3N_4 in the HPBR at 6 atm total pressure, 0.6 atm H_2O, and 20 m/s. The large square symbols at the highest and lowest temperature were obtained for times approaching 200h. Other exposures were typically 50h.
7. SEM image and EDS analysis of AS800 surface after exposure in the HPR at 1300°C, 6 atm total pressure, 0.6 atm H_2O, 20 m/s for 50h.
8. EM image and EDS analysis of SN282 surface after exposure in the HPR at 1225°C, 6 atm total pressure, 0.6 atm H_2O, 20 m/s for 102h.
9. SEM cross-sectional images of materials after exposure in the HPBR at 6 atm, 0.6 atm H_2O, 20 m/s. A) AS800, 1170°C, 50h. B) AS800, 1330°C, 196h. Arrows show peaks of silica exposed on the surface of the sample.

C) AS800, 1330°C, 196h. Arrows show cracks in La_2Si_2O7 phase. D) SN282, 1225°C, 102h.

10. Measured recession for trailing edges of AS800 and SN282 vanes exposed in the turbine engine.
11. SEM cross-sectional images of AS800 vanes after exposure in the turbine engine at 1066-1260°C, 8.7 atm, 0.9 atm H_2O, 160-570 m/s for A) 815h and B) 500h.
12. SEM cross-sectional images of SN282 vane after exposure in the turbine engine at 1066-1260°C, 8.7 atm, 0.9 atm H_2O, 160-570 m/s for 1148h.
13. Polymorphs of $RE_2Si_2O_7$ as a function of RE ionic radius. After Felsche [16].
14. Phase diagram for the La_2O_3-SiO_2 sytem. After Bondar [18].

A.

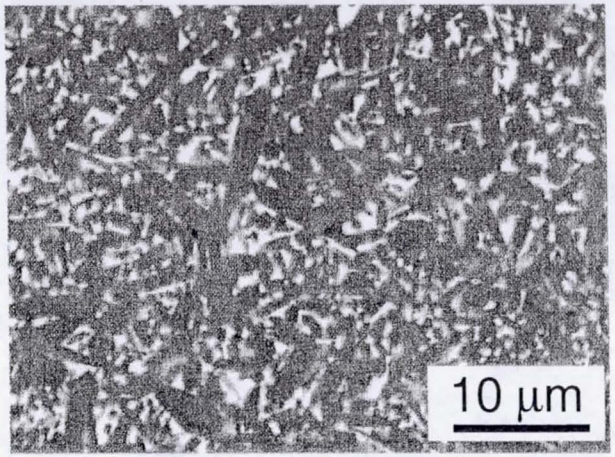

B.

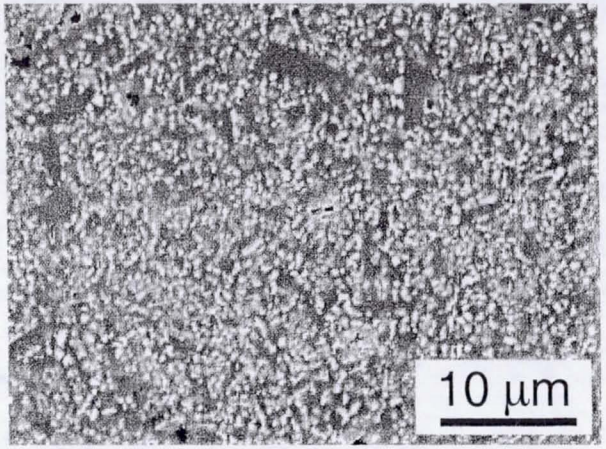

Figure 1. SEM inages of the as-received materials. A) AS800 B) SN282

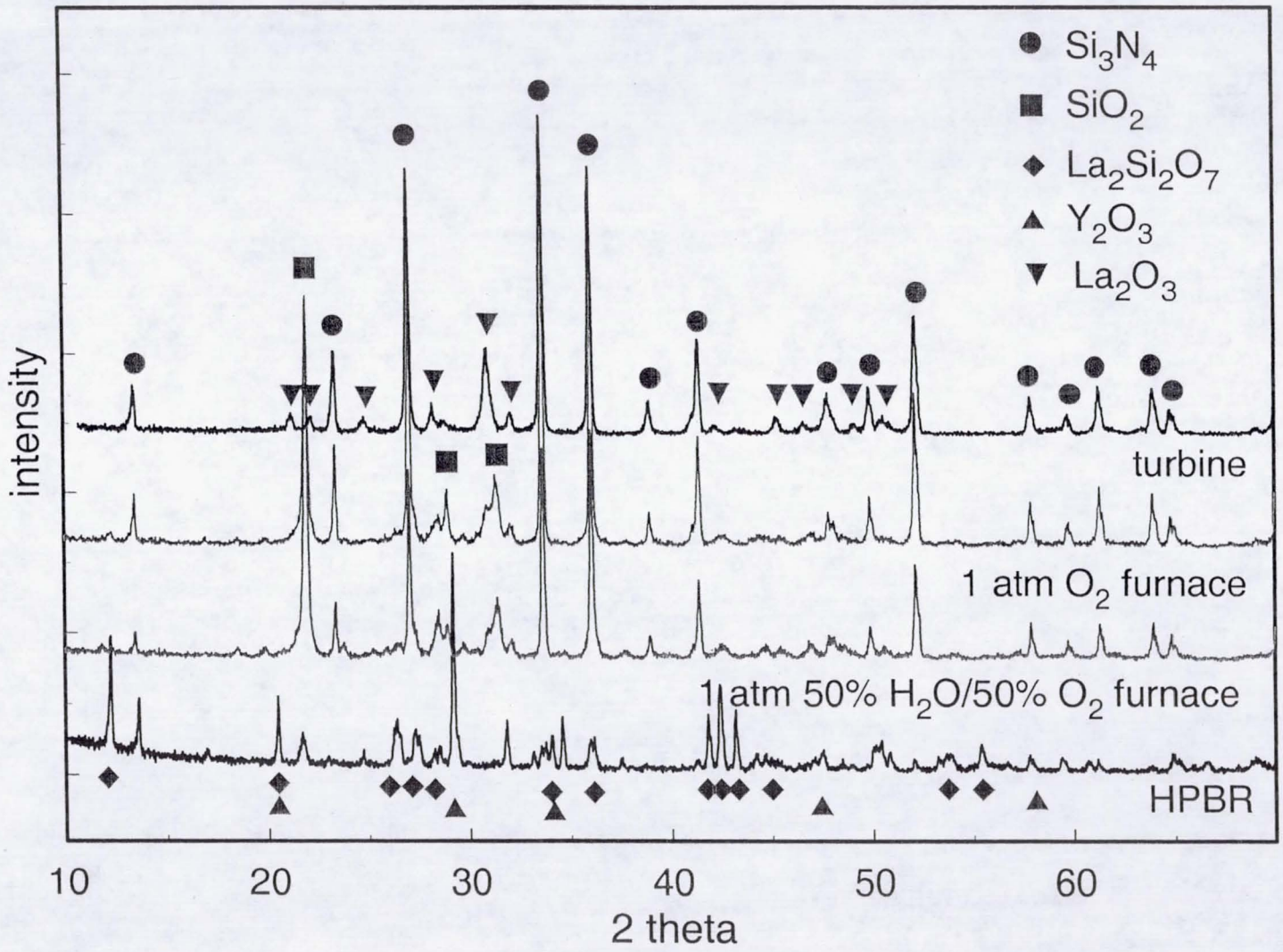

Figure 2. XRD spectra for AS800 exposed under various conditions. The O_2, H_2O and HPBR exposures were obtained at 1300°C. The turbine exposure was at temperatures between 1066 and 1260°C.

A.

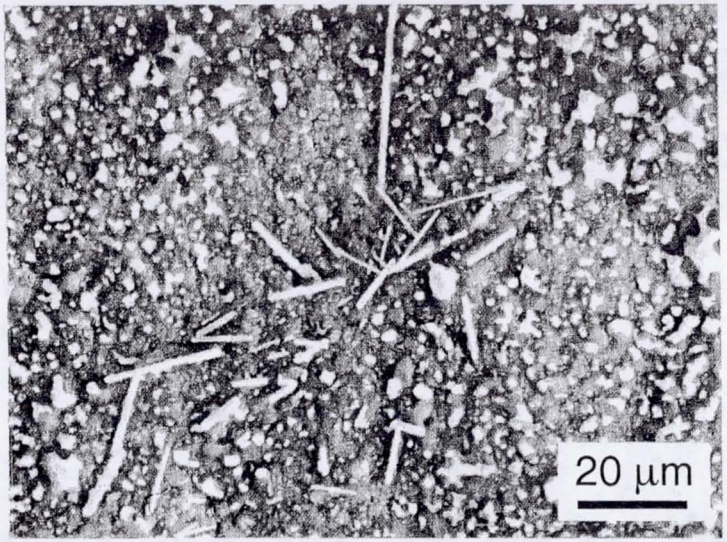

B.

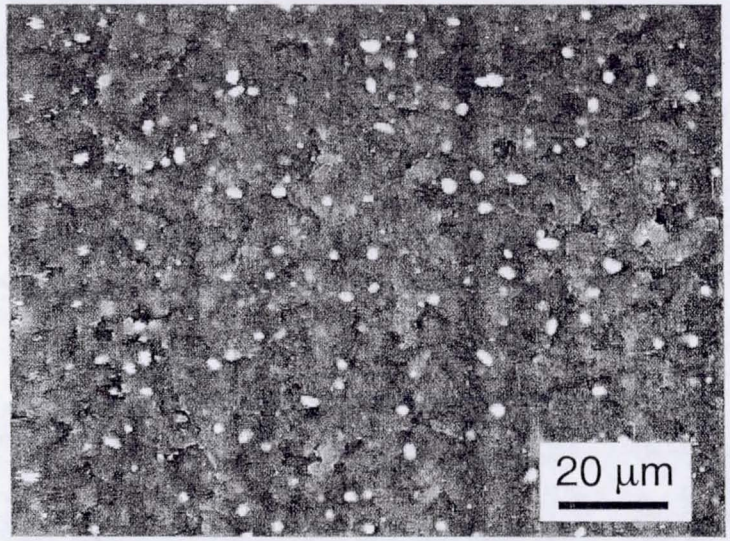

Figure 3. SEM images of AS800 (A) and SN282 (B) surfaces after exposure in dry oxygen at 1300°C for 100h.

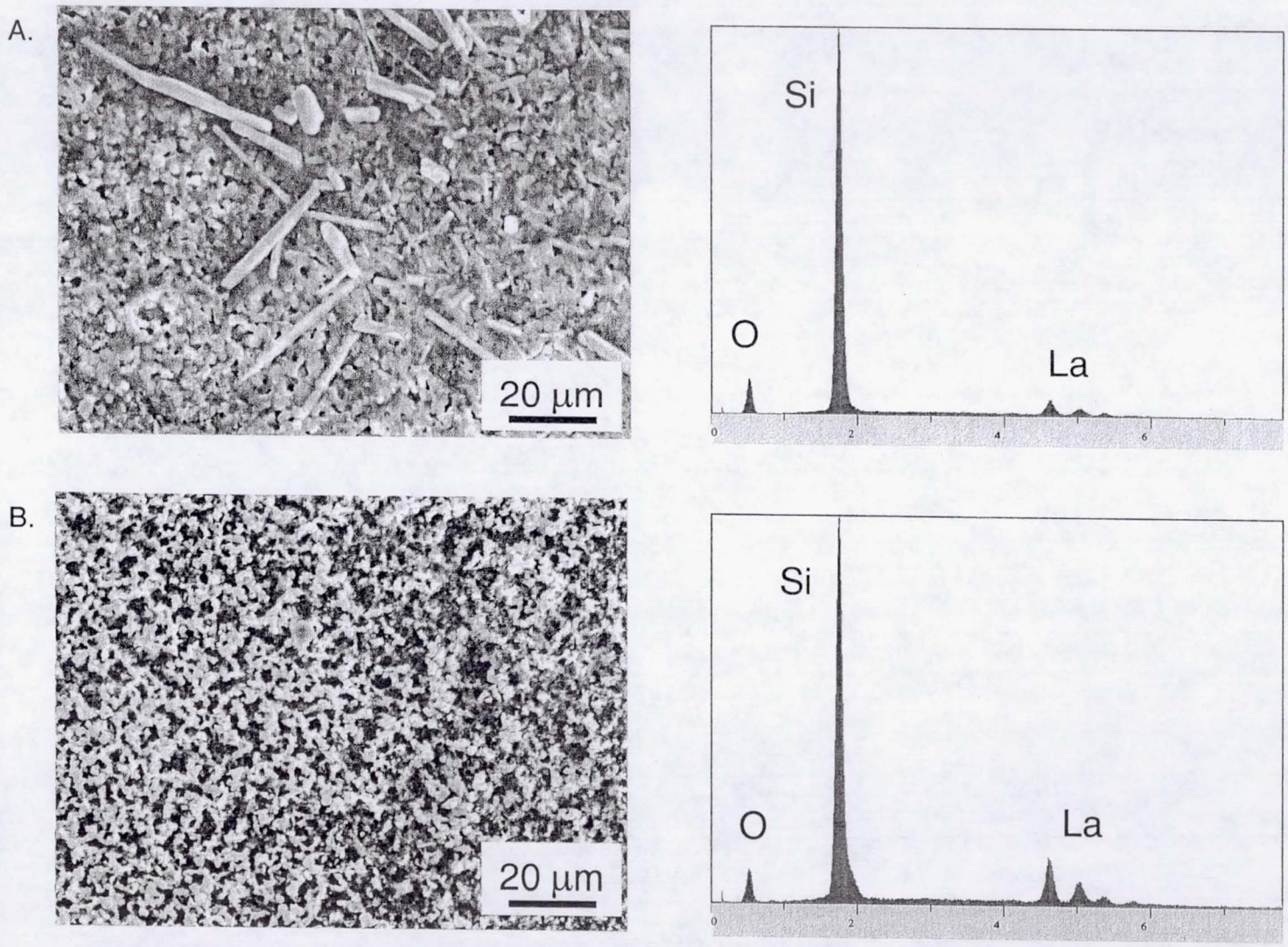

Figure 4. SEM images and corresponding EDS analyses of AS800 surfaces after exposure at 1300°C, 0.5 atm H_2O, 4.4 cm/s, 100h. (A) typical area (B) bottom of sample

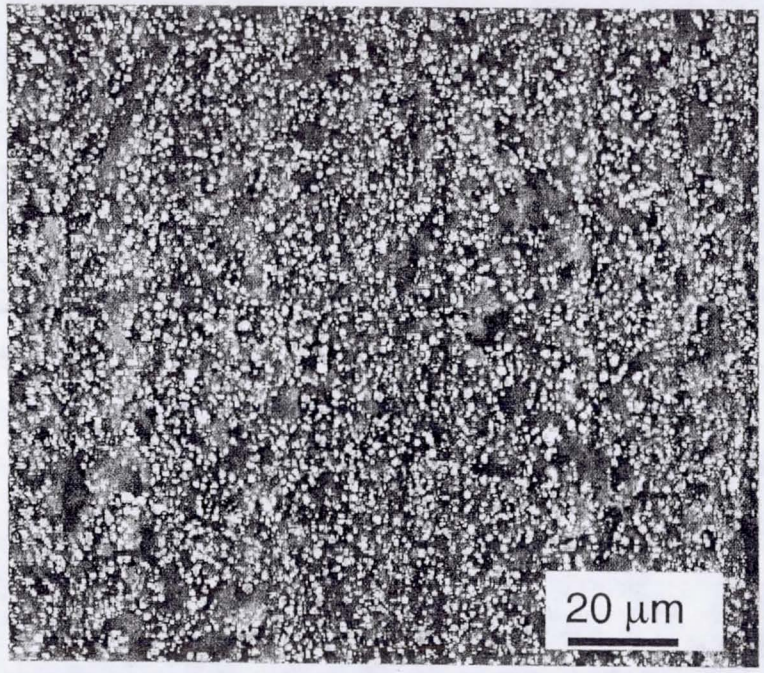

Figure 5. SEM image of SN282 surface after exposure at 1300°C, 0.5 atm H_2O, 4.4 cm/s, 100h.

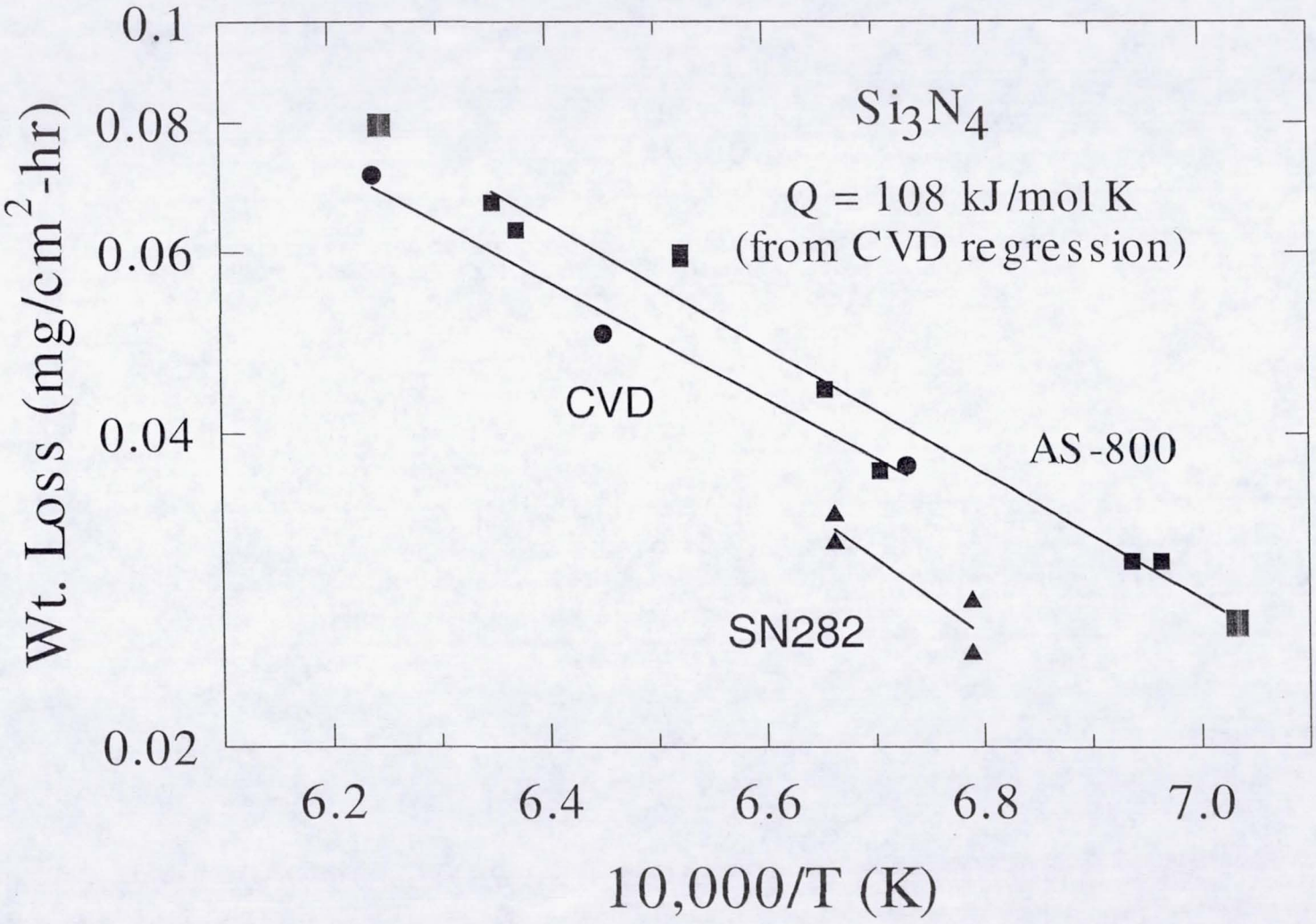

Figure 6. Weight loss rates obtained for Si_3N_4 in the HPBR at 6 atm total pressure, 0.6 atm H_2O, and 20 m/s. The large square symbols at the highest and lowest temperature were obtained for times approaching 200h. Other exposures were typically 50h.

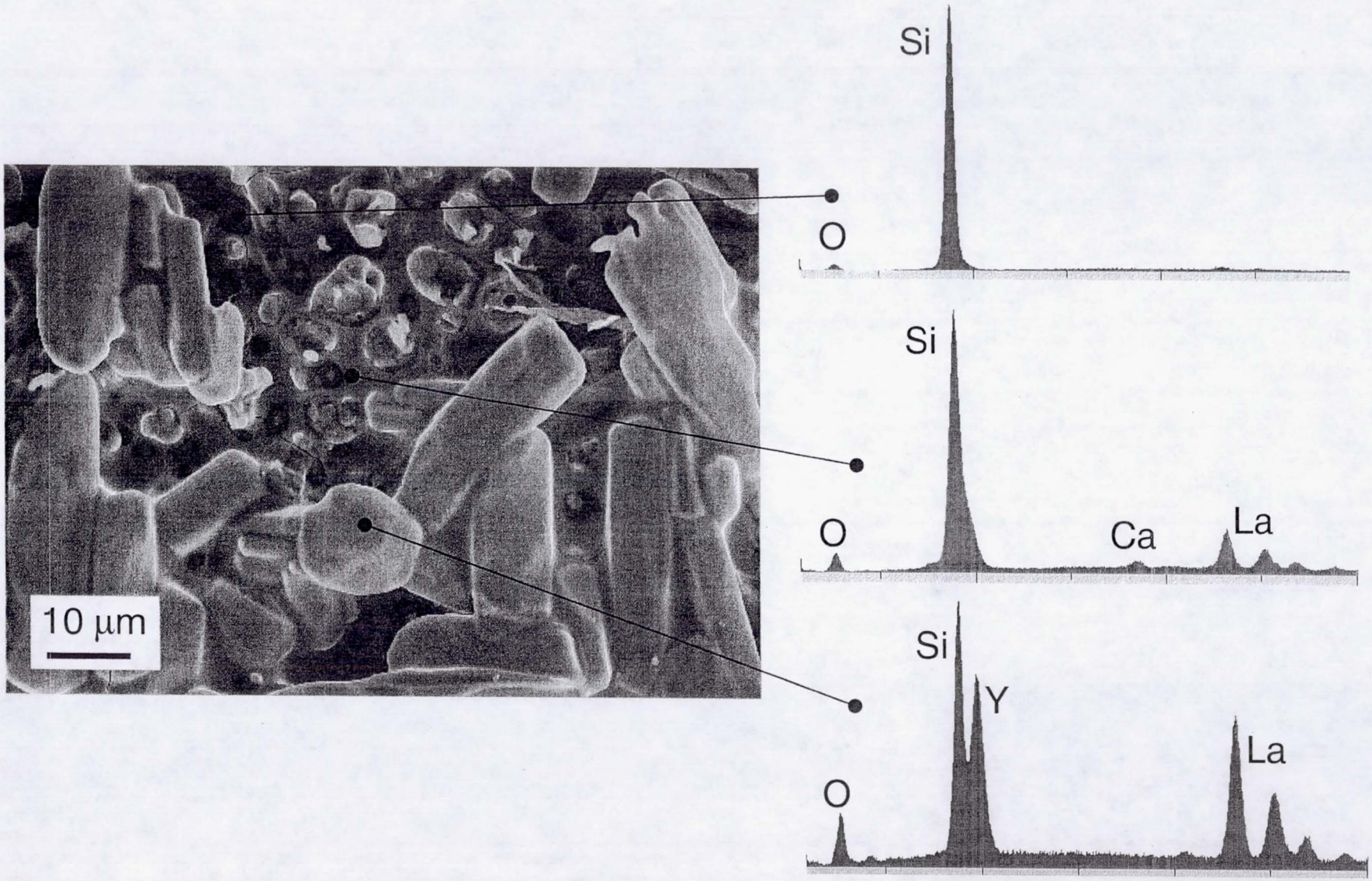

Figure 7. SEM image and EDS analysis of AS800 surface after exposure in the HPBR at 1300°C, 6 atm total pressure, 0.6 atm H_2O, 20 m/s for 50h.

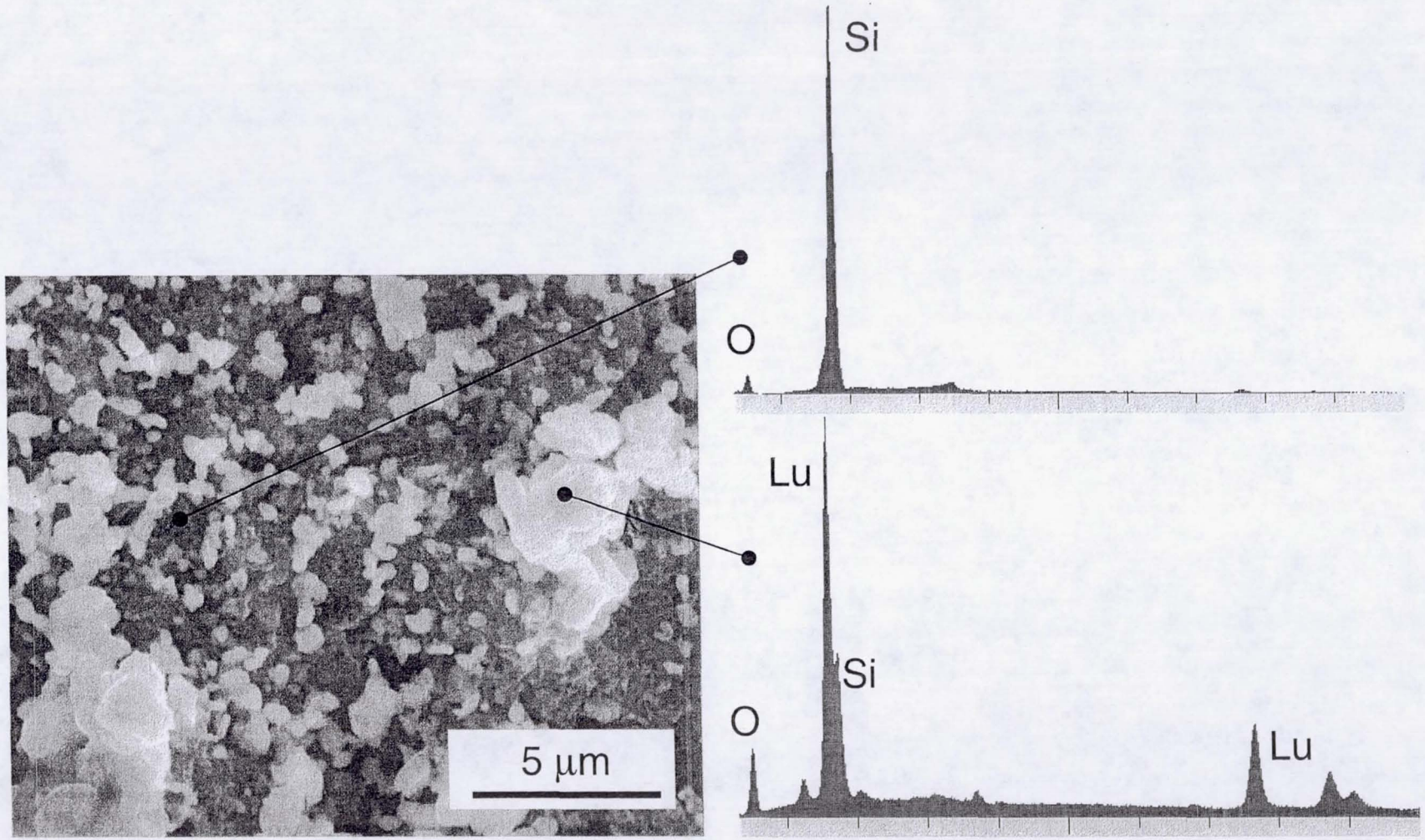

Figure 8. SEM image and EDS analysis of SN282 surface after exposure in the HPBR at 1225°C, 6 atm total pressure, 0.6 atm H_2O, 20 m/s for 102h.

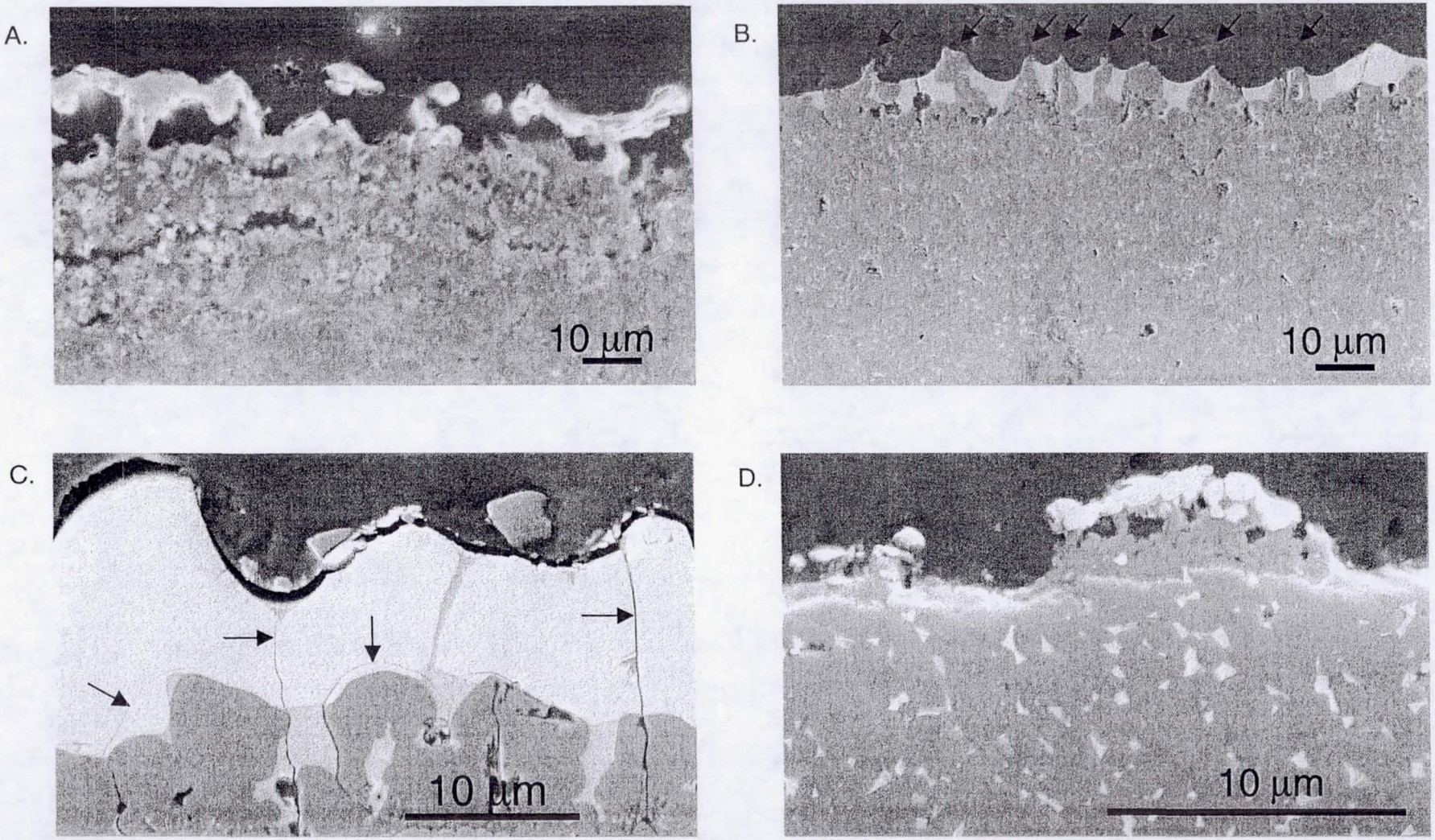

Figure 9. SEM cross-sectional images of materials after exposure in the HPBR at 6 atm, 0.6 atm H_2O, 20m/s. A) AS800, 1170°C, 50h. B) AS800, 1330°C, 196h. Arrows show peaks of silica exposed on the surface of the sample. C) AS800, 1330°C, 196h. Arrows show cracks in $La_2Si_2O_7$ phase. D) SN282, 1225°C, 102h.

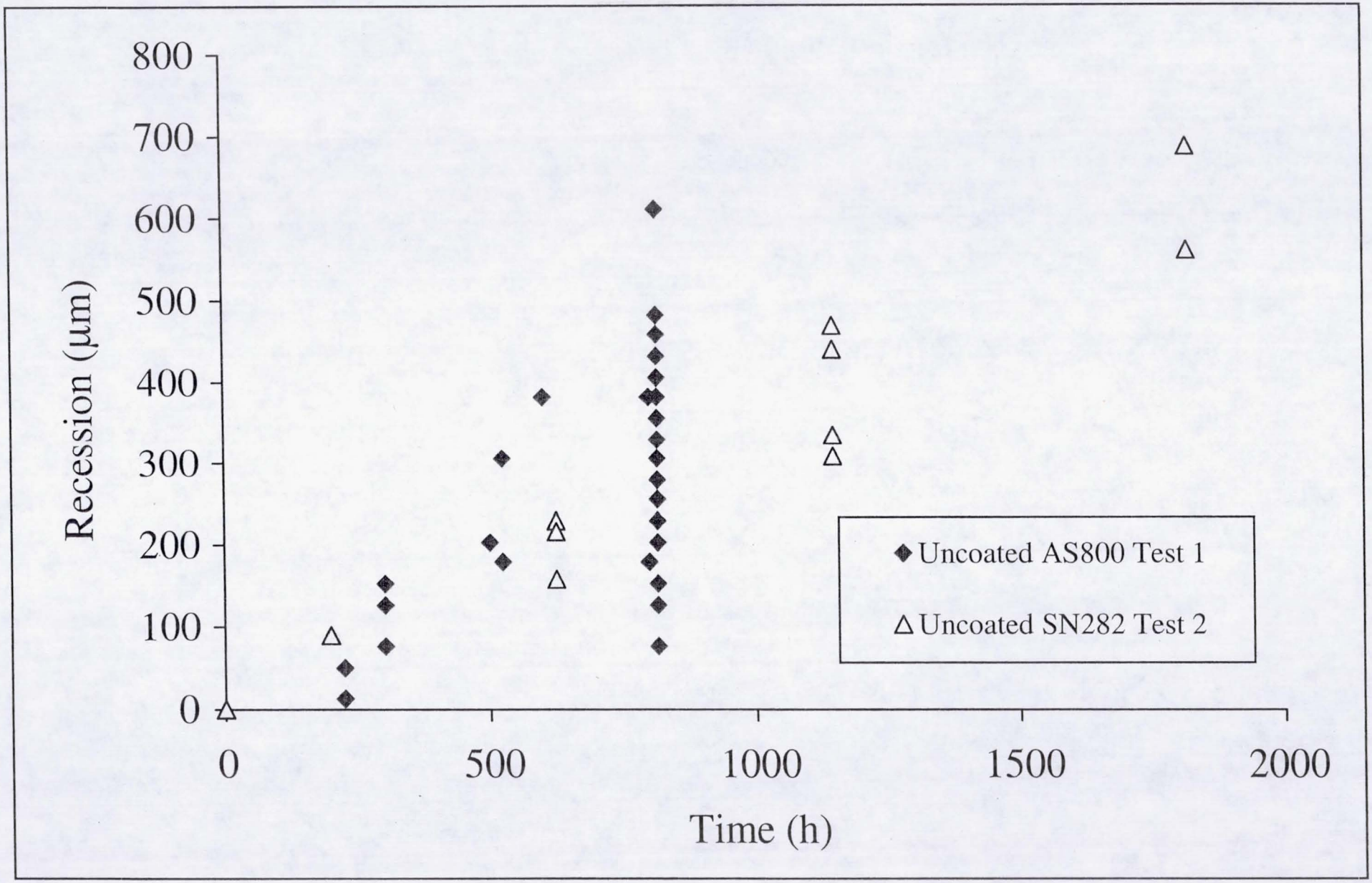

Figure 10. Measured recession for trailing edges of AS800 and SN282 vanes exposed in the turbine engine.

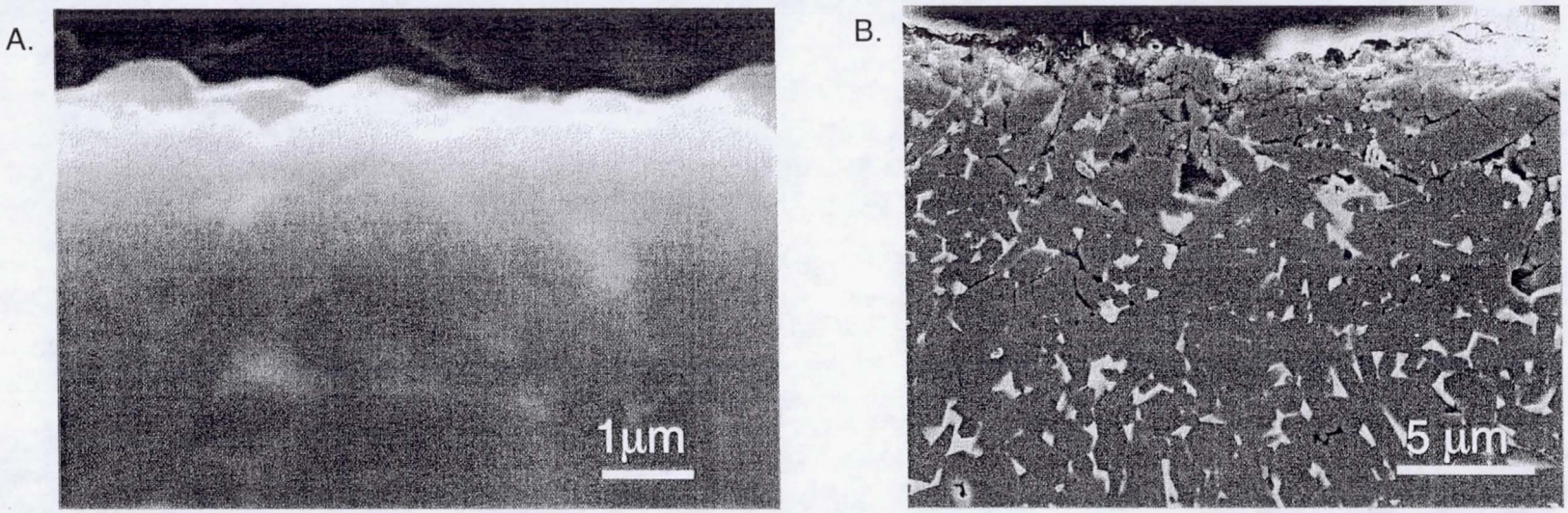

Figure 11. SEM cross-sectional images of AS800 vanes after exposure in the turbine engine at 1066-1260°C, 8.7 atm, 0.9 atm H_2O, 160-570 m/s for A) 815h and B) 500h.

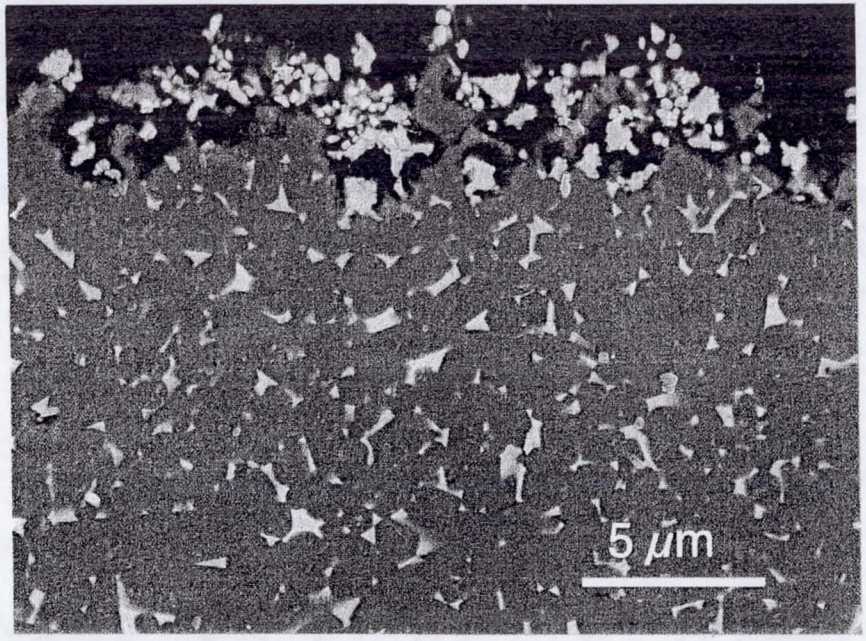

Figure 12. SEM cross-sectional images of SN282 vane after exposure in the turbine engine at 1066-1260°C, 8.7 atm, 0.9 atm H_2O, 160-570 m/s, for 1148h.

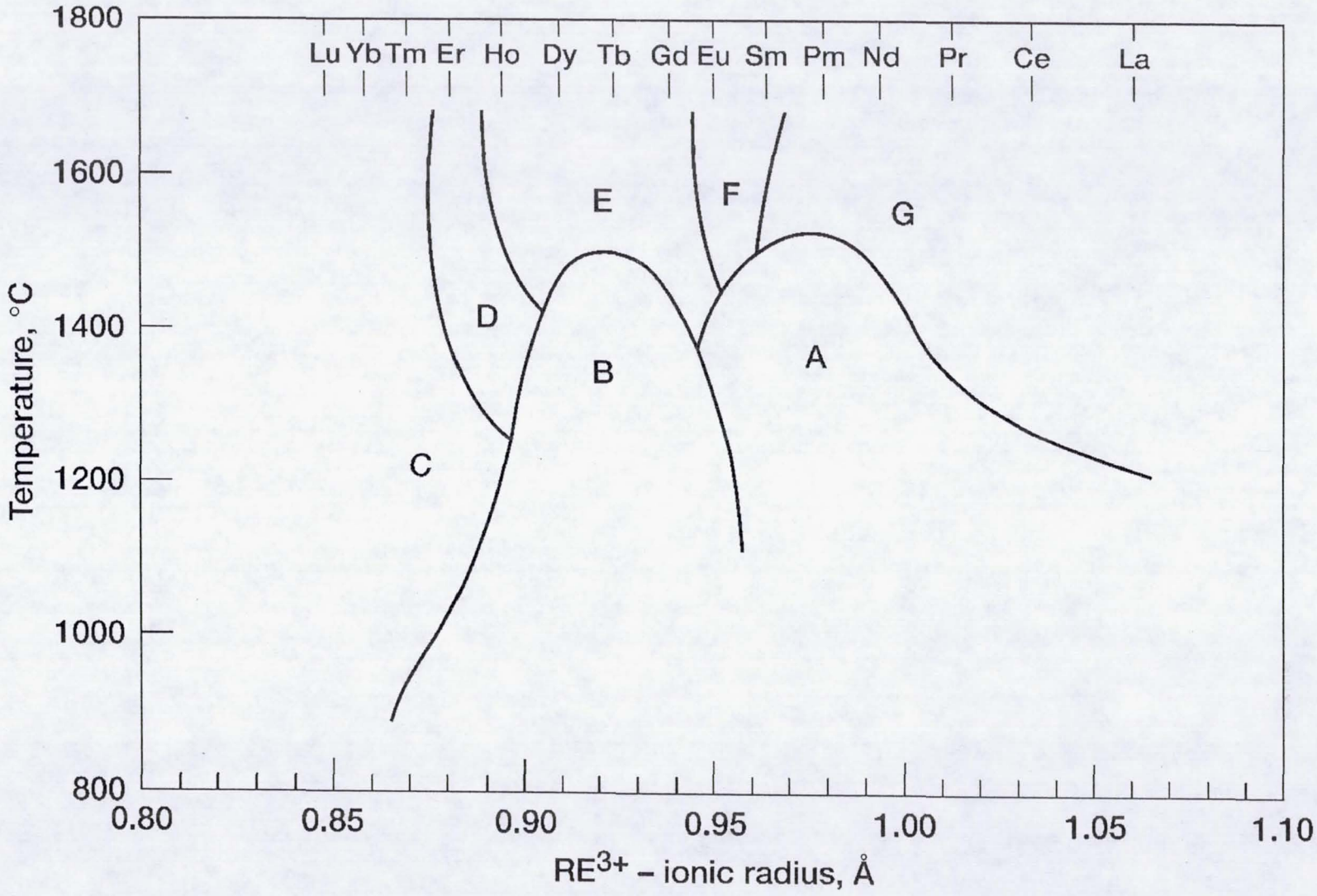

Figure 13. Polymorphs of $RE_2Si_2O_7$ as a function of RE ionic radius. After Felsche [16].

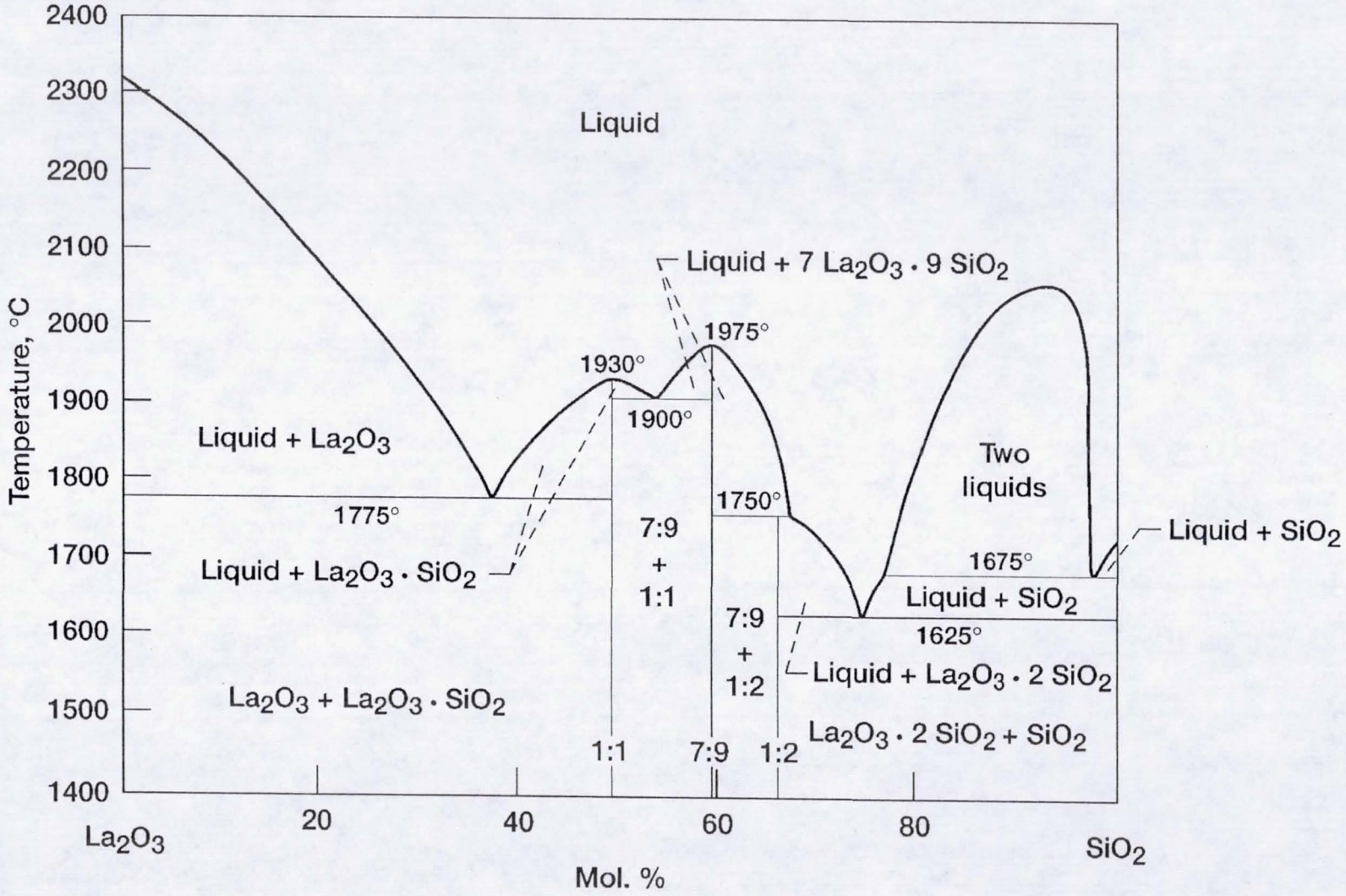

Figure 14. Phase diagram for the La_2O_3-SiO_2 system. After Bondar [18].